COMPARISON OF 1-D AND 3-D FINITE ELEMENT STRUCTURAL DYNAMICS MODELING

Hyeonsoo Yeo

Aeroflightdynamics Directorate (AMRDEC)
U.S. Army Research, Development, and Engineering Command
Ames Research Center, Moffett Field, CA, U.S.A.

Khiem-Van Truong

D.A.D.S.
ONERA
Châtillon, France

Robert A. Ormiston

Aeroflightdynamics Directorate (AMRDEC)
U.S. Army Research, Development, and Engineering Command
Ames Research Center, Moffett Field, CA, U.S.A.

ABSTRACT

Comparisons between 1-D and 3-D analyses are conducted systematically for advanced geometry blades which have tip sweep, tip taper, and planform variations near the root with various materials and effects of boundary conditions in order to better understand the differences between the two approaches and physics behind them. 1-D beam analysis is conducted using the RCAS rotorcraft comprehensive analysis with VABS calculated 2-D cross-sectional properties. 3-D finite element analysis is conducted using a commercial code MSC/Marc. Natural frequencies are calculated at various rotor rotational speeds and the differences are quantified. There is very good agreement between the 1-D and 3-D analyses for free-free aluminum beams, even for a very short beam with beam length five times chord (L = $5\times$c). The 1-D analysis accurately captures the planform variation near the root for an aluminum beam. In general, the differences between the 1-D and 3-D analyses occur when there is coupling, either generated from geometry (tip sweep) or material (composite), especially for high frequency modes. Without coupling, the 1-D analysis appears to capture free vibration characteristics of various advanced geometry beams and blades reasonably well for at least the six lowest frequency modes when the beam length is greater than ten times chord.

1. INTRODUCTION

Rotorcraft aeromechanics analysis is a challenging problem due to coupling of the complex structural deformations of rotor blades with the three dimensional and highly unsteady aerodynamic environment. Rotorcraft comprehensive analyses [1–5] have been widely used to model a broad spectrum of rotorcraft attributes, including performance, airloads, structural loads, air flow fields, and hub loads. Most rotorcraft comprehensive analysis codes use 1-D beam elements for rotor blade dynamics modeling. Traditional approaches rely on the fact that rotor blades are typically long slender structures with slowly varying elastic properties. This enables the use of 1-D beam theory for aeroelastic analysis. This method is efficient and accurate as long as the cross-sections are small compared to the wave-length of deformations along the beam. Modern rotor blades have begun to depart from simple straight planforms by incorporating tip sweep and taper. Cantilever (hingeless, bearingless rotors) blades involve planform and cross-section variations at the blade root. Use of composite material also complicates analysis due to material anisotropy [6]. Such configurations raise the question of validity of 1-D beam methods. More sophisticated structural models such as plates, shells, and brick elements will require increased computational effort. Therefore it is worth assessing the need for additional sophistication of 3-D analysis. Interested readers are referred to recent efforts to develop a parallel and scalable solution procedure for a 3-D finite element method (FEM) based rotor dynamics analysis [7] and to develop a geometrically exact 2-D shell element for rotorcraft comprehensive analysis [8, 9].

Truong calculated modal frequencies of ERATO blade (a French acronym for “Etude d’un Rotor Aéroacoustique Technologiquement Optimisé”) using both 3-D finite element analysis and 1-D beam analyses, and compared the results with experiment [10]. The 3-D finite element analysis was conducted using MSC/Marc and the 1-D analysis was conducted using MSC/Marc (beam model) and Eurocopter’s

aeroelastic code R85, which is a predecessor of the comprehensive helicopter aeroelastic code HOST [5]. The predicted modal frequencies using the 3-D analysis showed better correlation with the experiment than with the 1-D analyses. The findings of this study motivated the present cooperative research. The US Army Aeroflightdynamics Directorate (AFDD) and the French Office National d'Etudes et de Recherches Aérospatiales (ONERA) have conducted research to investigate the differences between a 1-D beam model approach and a 3-D finite element approach under the auspices of the United States/France Memorandum of Agreement on Helicopter Aeromechanics. The objective of this effort is to better understand the accuracy of current rotor blade structural modeling and identify the level of sophistication required to model modern rotor blades.

AFDD used a geometrically exact, shear flexible, anisotropic beam element implemented in the Rotorcraft Comprehensive Analysis System (RCAS). The new element, termed the RCAS geometrically exact composite beam (GCB) element [11], goes beyond the original RCAS nonlinear beam (NLB) element. The GCB element is specifically intended for composite blades and it is designed to be compatible with Variational Asymptotical Beam Sectional Analysis (VABS) [12], a code developed by Cesnik, Hodges, and their co-workers at Georgia Institute of Technology for determining beam cross-section elastic and mass constants. The development of RCAS GCB element assumed that the cross-sectional strain energy is given in terms of elastic constants. These can be calculated by finite-element-based cross-sectional analyses such as VABS. Thus, the strain energy is given in terms of certain elastic constants as they vary along the beam. The complete process includes creating a cross-section mesh, transforming that mesh to an input file format for VABS, running VABS, and inputting the VABS output file into the inertial and elastic property file for RCAS.

ONERA used commercial codes MSC/Marc for the 3-D finite element analysis and MSC/Patran for the generation of meshes using 3-D bricks, thick shells, and beams. MSC/Marc is a nonlinear finite element code that provides capabilities for studying dynamic structures undergoing large deformations and it includes both geometric and material nonlinearities. It is a general-purpose code for simulating a wide range of engineering applications and manufacturing processes.

This paper compares the state-of-the-art rotary wing structural analysis results with 3-D finite element results for beams and blades with various materials and geometries, and addresses the validity of 1-D beam analysis. Many previous studies were mostly devoted to development of beam theories and validation with limited experimental and 3-D analysis results. The most logical way to assess the limitation of 1-D beam theories for rotor blade application is to directly compare 1-D and 3-D modeling approaches for relevant blade geometries. The present authors systematically compared 1-D beam and 3-D analysis results for both isotropic and composite straight blades with various lengths and quantified the differences and also explored the adequacy of 3-D modeling assumptions and practices [13, 14]. As a continuation of previous work conducted by the present authors, this paper focuses on quantifying the differences between 1-D beam and 3-D finite element analysis for advanced geometry blades which have tip sweep, tip taper, and planform variations near the root. In addition to those, the effects of boundary condition are also examined for straight beams. Comparisons of natural frequencies at various rotor rotational speeds between the two analyses are conducted systematically to better understand the differences and physics behind them.

2. 1-D ANALYSIS

It will be useful to briefly discuss VABS and RCAS beam elements. A rotor blade has its length much greater than the other two dimensions and thus has often been treated as a beam, a 1-D structure, to reduce the computational costs associated with the analysis. In order to perform this idealization without loss of accuracy, one has to capture the behavior associated with the two omitted dimensions (the cross-sectional coordinates) by correctly accounting for the cross-sectional geometry and material distribution. VABS is able to calculate the one-dimensional cross-sectional stiffness constants, with transverse shear and Vlasov refinements, for initially twisted and curved beams with arbitrary geometry and material properties. The variational asymptotic method (VAM) developed by Berdichevsky [15] is the mathematical basis of VABS and is used to split a general 3-D nonlinear elasticity problem for a beam-like structure into a 2-D cross-sectional analysis and a 1-D nonlinear beam analysis. It allows one to replace a 3-D structural model with a reduced-order model in terms of an asymptotic series of certain small parameters inherent to the structure. These small parameters are a/l and a/R, where a is the characteristic length of the cross-section, l is the characteristic wavelength of deformation along the longitudinal direction, and R is the characteristic radius of the initial curvature and twist. The main small parameter for straight blades is a/l. As l corresponds to the characteristic wavelength of deformation, it will decrease as the mode number (n) increases, roughly proportional to L/n where L is the length of a beam. It is then expected that the accuracy of the 1-D theory deteriorates as a beam length becomes shorter, and especially for higher modes. VABS development and comparison with other composite beam theories are described in Refs. 16-21.

The generalized strain energy per unit length accounting for

transverse shear and trapeze effect is shown below;

$$U = \frac{1}{2}\begin{Bmatrix}\gamma_{11}\\ 2\gamma_{12}\\ 2\gamma_{13}\\ \kappa_1\\ \kappa_2\\ \kappa_3\end{Bmatrix}^T \begin{bmatrix} S_{11}\,S_{12}\,S_{13}\,S_{14}\,S_{15}\,S_{16}\\ S_{12}\,S_{22}\,S_{23}\,S_{24}\,S_{25}\,S_{26}\\ S_{13}\,S_{23}\,S_{33}\,S_{34}\,S_{35}\,S_{36}\\ S_{14}\,S_{24}\,S_{34}\,S_{44}\,S_{45}\,S_{46}\\ S_{15}\,S_{25}\,S_{35}\,S_{45}\,S_{55}\,S_{56}\\ S_{16}\,S_{26}\,S_{36}\,S_{46}\,S_{56}\,S_{66}\end{bmatrix} \begin{Bmatrix}\gamma_{11}\\ 2\gamma_{12}\\ 2\gamma_{13}\\ \kappa_1\\ \kappa_2\\ \kappa_3\end{Bmatrix}$$
$$+ \begin{Bmatrix}\gamma_{11}\\ \kappa_1\\ \kappa_2\\ \kappa_3\end{Bmatrix}^T (\gamma_{11}A+\kappa_1 B+\kappa_2 C+\kappa_3 D) \begin{Bmatrix}\gamma_{11}\\ \kappa_1\\ \kappa_2\\ \kappa_3\end{Bmatrix}$$

where γ_{11} is the extensional strain measure, $2\gamma_{12}$ and $2\gamma_{13}$ are the transverse shear strain measures of the cross-section, κ_1 is the elastic twist strain measure, and κ_2 and κ_3 are bending strain measures. This is referred to as a generalized Timoshenko model [19]. Assuming that the elastic constants are correctly determined, it is accurate as long as $a^3 \ll l^3$ and thus is more accurate than the classical model, particularly for the second and higher modes dominated by bending. Cross-sectional analyses are usually linear, but the "trapeze effect" is a nonlinear effect caused by extension-torsion coupling in beams undergoing large axial forces due to large centrifugal forces. It slightly increases the effective torsional stiffness and thus the rotating torsional frequencies. Reference 22 provides a more detailed description on how the trapeze effect is modeled in VABS.

The elements of the 6×6 inertial matrix are arranged as

$$\begin{bmatrix} \mu & 0 & 0 & 0 & \mu x_{m3} & -\mu x_{m2}\\ 0 & \mu & 0 & -\mu x_{m3} & 0 & 0\\ 0 & 0 & \mu & \mu x_{m2} & 0 & 0\\ 0 & -\mu x_{m3} & \mu x_{m2} & I_{22}+I_{33} & 0 & 0\\ \mu x_{m3} & 0 & 0 & 0 & I_{22} & -I_{23}\\ -\mu x_{m2} & 0 & 0 & 0 & -I_{23} & I_{33}\end{bmatrix}$$

where μ is mass per unit length, $(x_{m2}; x_{m3})$ is the location of mass center, I_{22} is the mass moment of inertia about x_2 axis, I_{33} is the mass moment of inertia about x_3 axis, I_{23} is the product of inertia.

The complete RCAS plus VABS analysis process includes creating a cross-section mesh, transforming that mesh to an input file format for VABS, running VABS, and inputting the VABS output file into the sectional property file for RCAS. The data needed by the 1-D analysis consists of the cross-sectional 6×6 stiffness matrix, and the cross-sectional inertia properties. In addition, if the trapeze effect is to be included, one needs the 4×4 A, B, C, and D matrices.

The original RCAS NLB element uses geometrically nonlinear (but not exact) equations for extension, twist, and bi-axial bending (total 4 variables). The trapeze effect is included, but there are no shear deformation variables. An ordering scheme is used to simplify the equations of motion. The order of several geometrical parameters describing the undeformed beam and the state of the beam's deformation is estimated in terms of a dimensionless parameter ε so that $\varepsilon^2 \ll 1$. All terms are retained in the kinetic and strain energies through $O(\varepsilon)$ relative to the leading terms. The GCB element is geometrically-exact, which means that there is no need for ordering schemes. The only approximations are in the formulation of the beam constitutive law, the discretization process, and the element quadrature. GCB element uses six primary variables, three force strain measures (extension and two transverse shear) and three moment strain measures (twist and two bending).

In RCAS, large motions of the beam are provided for both NLB and GCB elements by the motion of element frames that are rigidly attached to their parent elements at their root. Element deformations are defined with respect to the element frame and thus the elastic deformations in each element remain small if sufficient beam elements are used. The effectiveness of this approach in RCAS addressing both rigid and flexible body kinematics has been demonstrated in Ref. 23.

3. 3-D FINITE ELEMENT ANALYSIS

The finite element method (FEM) is a numerical technique for finding approximate solutions to partial differential equations. Two key ingredients in the finite element analysis are mesh discretization and interpolation. The geometry to be analyzed (continuous domain) is divided into smaller regions of finite dimensions called finite elements, connected at discrete points called nodes. The physical variables associated with the nodes are interpolated over the element, using polynomials whose order depends upon the number of nodes assigned to the element.

The quality of the mesh plays a key role in the accuracy of the results. One of the factors that can affect the quality of a mesh is aspect ratio. Aspect ratio is ratio of longest edge length to shortest edge length. Normally, finite elements provide more accurate answers when the aspect ratio is closest to 1. For the present modeling and analysis, it was kept below 5. For an accurate finite element analysis, users need to decide what type of finite element would be appropriate and how fine a mesh would be sufficient. Mesh convergence refers to the minimum element size required to ensure that the results of an analysis are not affected by

changing the size of the mesh. This is determined by the characteristic size (h) of the elements. This is called the h-refinement of the model. If the mesh is too coarse, the elements will not be able to capture the behavior of the structure and there would be a discretization error. On the other hand, if the mesh is too dense, solution time will be too high. An ideal mesh would use just enough elements to arrive at 100% convergence. The alternative to the h-refinement is increasing the order of the element shape functions (p-refinement).

MSC/Marc provides linear and quadratic elements for 3-D solids. The transformation from the linear elements to the quadratic elements can be done quasi-automatically with the graphic interface MSC/Marc Mantat. MSC/Marc also offers a wide range of element libraries including 3-D solid elements (8-noded and 20-noded hexahedrons, and 4-noded and 10-noded tetrahedrons, etc.) and various shell elements. It is interesting to note that the choice of elements is sometimes dictated by the problem considered. For instance, if aerodynamic nodal forces and moments are applied into the 3-D structure, there is no other alternative than using shell elements for modeling the blade skin, as the nodes of solid elements have only translational degrees of freedom and do not carry moments.

MSC/Marc also can be tailored to user needs through user defined subroutines written in Fortran. Furthermore, it has parallel analysis capabilities for all the steps of analysis (assembly, matrix solution, and stress recovery). MSC/Marc has been successfully coupled with comprehensive helicopter aeroelastic code HOST and computation fluid dynamics (CFD) code for rotorcraft aeromechanics analysis [24]. 3-D finite element modeling assumptions and practices relevant to the present study can be found in Ref. 14.

4. RESULTS AND DISCUSSION

Comparisons between the 1-D and 3-D analyses are conducted systematically for several problems to better understand the differences and physics behind them. First, effects of boundary condition are examined. Then, effects of tip sweep, tip taper, and planform variation near the blade root are investigated. It should be noted that both RCAS NLB element and GCB element are used for the investigation of boundary condition, however, only RCAS GCB element is used for the remaining analyses.

4.1. Effects of boundary condition and beam length

Natural frequencies were calculated for an aluminum solid section beam using 1-D and 3-D analyses. Figure 1 shows the geometry of the beam investigated. The beam is clamped to the wall at the root. The width of the cross-section is 3.4-in and the thickness is 0.85-in and the length of the beam is twenty times chord (20×c) and ten times chord (10×c). The Young's modulus is E = 1.0E+07 lb/in^2, Poisson's ratio is ν = 0.3, and the mass density is ρ = 2.538E-04 lb sec^2/in^4.

RCAS uses 30 elements for L = 20×c and 15 elements for L = 10×c. The cross-sectional properties were obtained from VABS using 9-noded quadrilateral elements. It should be noted that 6×6 mass and stiffness matrices can be generated analytically for a homogeneous, isotropic, solid rectangular cross-section. The two methods produced the same cross-sectional properties. For the 1-D analysis, the clamped boundary condition was applied by zeroing all the six variables (three displacements and three rotations) at the root node. In the 3-D finite element analysis, the beam is modeled by brick elements as shown in Fig. 2. For the 3-D analysis, the clamped boundary condition was applied as follows. First, all the nodes at the cross-section at the root are connected to the center node through rigid links using rigid body element RBE2 in MSC/Marc as shown in Fig. 2. Then, the clamped boundary condition was applied by zeroing three displacement degrees of freedom of the center node. Thus, the clamped boundary conditions modeled by the 1-D and 3-D analyses are not exactly same.

Figure 3 shows the natural frequencies calculated from both RCAS and MSC/Marc. Comparisons are made for up to 8 modes in this figure and throughout the paper. With beam length 20×c, there is good agreement between the two analyses for low frequency modes and most of high frequency modes, except the fifth flap mode. As expected, the rotational speed increases the flap frequencies due to centrifugal force, but has a small influence on the lag and torsion frequencies. As the beam length is reduced to 10×c, there is a significant increase in frequencies as would be expected. According to classical beam theory, non-rotating flap and lag frequencies are proportional to 1/L^2 and torsion frequencies to 1/L. The 1-D beam analysis results deviate from the 3-D analysis calculations as the beam length becomes 10×c and the effects of 3-D characteristics become more important. There is still good agreement between the two approaches for lower modes, however, the differences become larger for higher modes.

As previously mentioned, there is a difference in the boundary condition that constrains the clamped end of the beam between the 1-D and 3-D analyses. In order to understand the effects of boundary condition on the natural frequency calculation, free-free beam analysis is conducted. This will eliminate any uncertainties associated with the boundary condition. Table 1 compares non-rotating (zero RPM) first torsion frequencies of clamped-free and free-free beams with various beam length. The cross-section geometry is same as the one in Fig. 1. Analytical solutions can be found for clamped-free Euler-Bernoulli beam as $\omega_{T1} = \frac{1}{2}\frac{\pi}{L}\sqrt{\frac{GJ}{I}}$, where GJ is torsional stiffness and I is moment of inertia, and the effective length is reduced by half for the free-free beam. And thus the L = 20×c results for the free-free beam

are identical to the L = 10×c results for the clamped-free beam. Both RCAS NLB element and GCB element are used to compare the capabilities of the two elements. RCAS results are exactly same as the analytical solutions. The first torsion frequency of the free-free beam of length L is identical to that of the clamped-free beam of length L/2 as the mid-span of the free-free beam acts as a clamped boundary. The 3-D results are quite different from the 1-D results for the clamped-free case, and the difference gets larger as the beam length decreases. However, they are very close to the 1-D results for the free-free beam. Unlike the 1-D results, the first torsion frequency of the free-free beam of length L is not same as that of the clamped-free beam of length L/2. The mid-span of the free-free beam experiences warping of the cross section, while it was constrained for the clamped condition.

The non-rotating third flap frequencies are compared for the same beam in Table 2. Again, the analytical solution was obtained for the Euler-Bernoulli beam as $\omega_{F3} = (7.855)^2\sqrt{\frac{EI}{mL^4}}$, where EI is flap stiffness and m is mass per unit length, for the clamped-free boundary condition and $\omega_{F3} = (10.996)^2\sqrt{\frac{EI}{mL^4}}$ for the free-free boundary condition. The NLB elements, which include nonlinear terms, reduce frequencies compared to the results with the classical Euler-Bernoulli beam theory. With the inclusion of shear flexibility, the GCB elements further reduce frequencies for higher frequency modes and shorter beams, and show better agreement with the 3-D results, especially for L = 5×c case. Again, there is better agreement for the free-free beam than the clamped-free beam between the two analyses.

4.2. Effects of tip sweep

This section investigates the effects of tip sweep with aluminum and composite beams and a more realistic rotor blade. Good experimental data for fundamental validation of swept tip blade frequencies were scarce until rotating beam data were obtained in the University of Maryland vacuum chamber [25]. This experiment included composite as well as aluminum beams, and those results are used for comparison. Figure 4 shows the geometry of the aluminum beam, which has been tested in the University of Maryland vacuum chamber. The length of the beam tested is L = 40-in, which included a 2.5-in hub. The width of the cross-section is 1.0-in and the thickness is 0.063-in.

Figure 5 shows the natural frequencies of aluminum beam with various tip sweep angles. The calculated results are compared with experimental data. Experimental frequency measurements were made up to 750 RPM. However, analytical calculations are extended to 1500 RPM. An RCAS model of the beam was developed with 20 elements to represent the beam section and 5 elements to represent the tip. Without tip sweep, both 1-D and 3-D analyses show identical results and good agreement with the experiment. As the sweep angle increases, strong coupling between flap and torsion occurs. The tip sweep has virtually no influence on the first flap and first lag mode frequencies, however, the coupling eliminates pure torsion and tends to reduce flap (flap dominant but coupled flap-torsion mode) frequencies as the sweep angle increases, especially at higher rotor speeds, and increase torsion frequency. The torsion frequency is not shown for the swept-tip cases as it is above the eighth mode (second lag mode became the eighth mode), but later plots on composite beams will show the trend clearly. For the 30-deg tip sweep, the two analyses show almost identical results up to about 1000 RPM, after that the 1-D beam analysis results deviate from the 3-D analysis calculations for the high frequency modes. The biggest differences between the two analyses occur for the eighth mode at the highest rotor speed and those are 0.11%, 1.48%, 3.29% for the 0-deg, 30-deg, and 45-deg sweep angles, respectively.

Figure 6 shows the natural frequencies for graphite-epoxy solid section beams with layup angle of $[0^\circ]_{24}$. The width of the cross-section is 1.0-in, same as the aluminum beam tested. However, the thickness of the cross-section is 0.117-in. The material properties [26] are: E_{11} = 2.059E+07 lb/in^2, $E_{22} = E_{33}$ = 1.42E+06 lb/in^2, $G_{12} = G_{13}$ = 8.9E+05 lb/in^2, G_{23} = 8.0E+05 lb/in^2, $\nu_{12} = \nu_{13}$ = 0.42, ν_{23} = 0.54, and ρ = 1.44E-04 lb sec^2/in^4. It should be noted that these beams are coupled only through tip sweep similar to the aluminum beams. Both 1-D and 3-D analyses show almost identical results and good correlation with the experiment without tip sweep. Again, the coupling decreases flap frequencies and increases torsion frequencies. As the sweep angle increases, more differences are observed for the high frequency modes. The differences between the two analyses are about 4.9% for the first torsion and second lag modes for the 45-deg sweep angle.

Figure 7 shows the natural frequencies for graphite-epoxy solid section beams with layup angle of $[15^\circ]_{24}$. the width of the cross-section is 1.0-in, same as the aluminum beam tested. However, the thickness of the cross-section is 0.127-in. It should be noted that there is flap-torsion coupling due to angle-ply lay-up for the $[15^\circ]_{24}$ case even without tip sweep. Unlike the previous two cases, a small difference was observed for the fifth flap mode even without tip sweep. The difference for the eighth mode frequency becomes larger as the sweep angle increases and RPM increases. It is interesting to note that the large difference in the second lag mode observed for the layup angle of $[0^\circ]_{24}$ with the 45-deg sweep angle did not occur for this case.

Natural frequencies are calculated for a realistic rotor blade with composite construction. The blade examined is a Mach-scaled hingeless rotor with straight and swept-tip blades tested in the U.S. Army Aeroflightdynamics Directorate (AFDD) 7- by 10-Foot Wind Tunnel in order to study aeroelastic phenomena [27]. These rotors are also referred as Advanced Dynamics Model (ADM). The objective of

this investigation is to compare the 1-D and 3-D approaches for the cross-section of a realistic composite blade, thus rotor blade flexure region was modeled rigid to simplify the analysis and some of the unknown material properties were assumed.

The planform used for the current analysis is shown in Fig. 8 and the cross-section is shown in Fig. 8(c). The width of the cross-section is 3.4-in. The materials and geometric information used for the individual components of the blade are in Ref. 13 and detailed cross-sectional material properties are listed in Table 3. Figure 9 compares natural frequencies calculated for the straight and 28-deg swept-tip ADM blades. Considering the complex geometry and materials and relatively short length, the results show very good agreement without tip sweep. For the 28-deg tip sweep, the two analyses show good agreement up to the sixth mode. However, there is a significant difference in the seventh and eighth modes. While the frequency of the seventh mode identified by 3-D analysis as flap-dominant mode increases as rotor speed increases, the 1-D results are insensitive to the rotor speed and it is identified as pure torsion mode by the 1-D analysis. Further investigation is needed to identify the source of the differences.

4.3. Effects of tip taper

This section investigates the effects of tip taper with an aluminum beam. Figure 10 shows the geometry of the beam. The baseline (without taper) geometry is same as the one in Fig. 1 and taper starts at 75% of the span and chord is reduced by 20% at the tip. Figure 11 shows the natural frequencies calculated from both RCAS and MSC/Marc for two different lengths. As there is no test data available on a beam with tip taper, only analysis results are compared. Flap frequencies did not change much from the baseline (without tip taper) results shown in Fig. 3. For the L = 20×c case, the first and second lag frequencies increased by 4.18% and 2.23%, respectively, compare to those of the straight (no taper) beam. And the first torsion frequencies increased by 6.60%. There is good agreement between the two analyses for the L = 20×c case, but the difference increases for the shorter L = 10×c case, especially for the high frequency modes. In general, moderate taper has a small influence on the natural frequencies for the geometry examined. Detailed modeling of more general tapered beam can be found in Ref. 28. Although the effects of tip taper on natural frequencies are small, cross-section variations near the blade root might play an important role. Thus, the chord variation near the blade root is examined in the next section.

4.4. Effects of planform variation near blade root

This section investigates the effects of planform variation near the blade root. Figure 12 shows the geometry of the beam. The length of the beam is L = 20×c, which included a 5%L hub. The width of the inboard flexure area is 0.4-in and the width of the main blade part is 2.4-in. There is a linear transition between the two sections from 12%L to 22%L span. The thickness is constant (0.24-in) from the root to tip. Detailed 3-D meshing is shown in Fig. 13. About 17000 elements are used for modeling the blade including about 4100 elements for the transition zone, which means about 25% of the total elements are devoted to the 10% of the blade length. Figure 14 shows the natural frequencies of aluminum beam with inboard transition zone. For the 1-D analysis, convergence study was conduced to identify sufficient number of elements to capture the geometric variations near the root. Figure 14(a) shows RCAS with 12 elements; 1 element in flexure, 1 in transition zone, and 10 in main blade. Figure 14(b) shows RCAS with 30 elements; 4 elements in flexure, 16 in transition zone, and 10 in main blade. There is a significant improvement in the 1-D analysis results by using more elements in the flexure and transition zone and the results from the two analyses show very good agreement.

Figure 15 plots first torsion and second lag frequencies calculated with RCAS with increasing number of elements in the flexure and transition zone. The numbers above each bar represent number of elements in the flexure and transition zone, respectively. As the number of elements increases, the frequencies decrease as expected. The 4 elements in the flexure and 16 in the transition zone is regarded as converged because using 32 elements in the transition zone changed the frequencies only less than 0.2%. It should also be mentioned that 8 elements in the flexure made virtually no influence.

Figure 16 shows the natural frequencies of graphite-epoxy solid section beams with layup angle of $[15^\circ]_{24}$. The planform and cross-section geometry are same as the one in Fig. 12. Again, RCAS results with both 12 elements and 30 elements are compared with the 3-D results. The two analyses show good agreement up to the sixth mode when 30 elements are used for the 1-D analysis (the difference is about 1% for the sixth mode at 1500 RPM). Among the seventh to ninth modes (ninth mode is not shown), the modal frequency lines cross each other around 850 RPM and 1000 RPM and the differences between the two analyses are larger around those RPMs. Using 32 elements in the transition zone did not improve the results.

5. SUMMARY AND CONCLUSIONS

Results from 1-D beam analysis using the RCAS rotorcraft comprehensive analysis with VABS calculated 2-D sectional properties are compared with 3-D finite element analysis using MSC/Marc to assess the validity of 1-D beam theories for rotor blade application. Natural frequencies are compared for free-free beams and advanced geometry blades which have tip sweep, tip taper, and planform variations near the root with various materials. Comparisons between the 1-D and 3-D analyses are made up to eight modes at various rotor rotational speeds for various beam lengths.

From this study the following conclusions were obtained:

1. There is very good agreement between the 1-D and 3-D analyses for free-free aluminum beams. The differences in the first torsion and third flap frequencies are 0.75% and 1.03%, respectively, for a very short beam with L = 5×c, which are much smaller than the differences for the clamped-free beams. RCAS geometrically exact composite beam (GCB) element includes shear flexibility, and thus produces better results compared to the conventional nonlinear beam (NLB) element for high frequency bending modes.

2. The 1-D and 3-D analyses show identical results and good agreement with the experiment for both aluminum and composite beams when the beam is sufficiently long and has no sweep. However, the differences between the 1-D and 3-D analyses increase as the tip sweep angle increases, especially for high frequency modes.

3. There is excellent agreement for the realistic composite blade (ADM blade) between the 1-D and 3-D approaches without tip sweep, considering very complicated layups. However, there are significant differences in the seventh and eighth modes for the swept-tip case. Especially the difference in the modal content for the seventh mode is not understood and further investigation is needed to identify the source of the difference.

4. In general, taper has a small influence on the natural frequencies for the geometry examined (taper starts at 75% of the span and chord is reduced by 20% at the tip). The differences between the two analyses did not change much due to the tip taper.

5. The 1-D analysis accurately captures the planform variation near the root for an aluminum beam when sufficient number of elements is used. However, the differences between the two analyses are larger for the composite beam with bending-torsion coupling.

6. In summary, the differences between the 1-D and 3-D analyses occur when there is coupling, either generated from geometry (tip sweep) or material (composite), especially for high frequency modes. Without coupling, the 1-D analysis appears to capture free vibration characteristics of various advanced geometry beams and blades reasonably well for at least the six lowest frequency modes when the beam length is greater than ten times chord.

6. ACKNOWLEDGMENTS

The first and third authors would like to express thanks to Dr. Jimmy Ho at Science and Technology Corporation, Ames Research Center and Prof. Dewey Hodges at Georgia Institute of Technology for sharing their experience and knowledge, especially Dr. Jimmy Ho for conducting the VABS analysis for the ADM blade.

References

[1] Saberi, H. A., Khoshlahjeh, M., Ormiston, R. A., and Rutkowski, M. J., "RCAS Overview and Application to Advanced Rotorcraft Problems," AHS Fourth Decennial Specialists' Conference on Aeromechanics, San Francisco, CA, Jan. 21-23, 2004.

[2] Johnson, W., "Rotorcraft Dynamics Models for a Comprehensive Analysis," AHS International 54th Annual Forum Proceedings, Washington, D.C., May 20-22, 1998.

[3] Bauchau, O. A., and Kang, N. K., "A Multibody Formulation for Helicopter Structural Dynamic Analysis," *Journal of the American Helicopter Society*, Vol. 38, No. 2, Apr. 1993, pp. 3-14.

[4] Bir, G., and Chopra, I. "University of Maryland Advanced Rotor Code (UMARC) Theory Manual," Technical Report UM-AERO 94-18, Center for Rotorcraft Education and Research, University of Maryland, College Park, MD, July 1994.

[5] Dequin, A. M., Benoit, B., Kampa, K., von Grünhagen, W., Basset, P. M., and Gimonet, B., "HOST, a General Helicopter Simulation Tool for Germany and France," American Helicopter Society 56th Annual Forum, Virginia Beach, VA, May 2-4, 2000.

[6] Jung, S. N., Nagaraj, V. T., and Chopra, I, "Assessment of Composite Rotor Blade Modeling Techniques," *Journal of the American Helicopter Society*, Vol. 44, No. 3, July 1999, pp. 188-205.

[7] Datta, A., and Johnson, W., "Three-dimensional Finite Element Formulation and Scalable Domain Decomposition for High Fidelity Rotor Dynamic Analysis," *Journal of the American Helicopter Society*, Vol. 56, No. 2, Apr. 2011, pp. 1-14.

[8] Bauchau, O. A., Choi, J. Y., and Bottasso, C. L., "On the Modeling of Shells in Multibody Dynamics," *Multibody System Dynamics*, Vol. 8, No. 4, 2002, pp. 459-489.

[9] Kang, H., Chang, C., Saberi, H., and Ormiston, R. A., "Assessment of Beam and Shell Elements for Modeling Rotorcraft Blades," American Helicopter Society 68th Annual Forum, Fort Worth, TX, May 1-3, 2012.

[10] Truong, V. K., "Dynamics Studies of the ERATO Blade, Based on Finite Element Analysis," 31st European Rotorcraft Forum, Florence, Italy, Sept. 13-15, 2005.

[11] Hodges, D. H., Saberi, H., and Ormiston, R. A., "Development of Nonlinear Beam Elements for Rotorcraft Comprehensive Analyses," *Journal of the American Helicopter Society*, Vol. 52, No. 1, Jan. 2007, pp. 36-48.

[12] Cesnik, C. E. S. and Hodges, D. H., "VABS: A New Concept for Composite Rotor Blade Cross-Sectional Modeling," *Journal of the American Helicopter Society*, Vol. 42, No. 1, Jan. 1997, pp. 27-38.

[13] Yeo, H., Truong, K., and Ormiston, R. A., "Assessment of 1-D Versus 3-D Methods for Modeling Rotor Blade Structural Dynamics," 51st AIAA/ASME/ASCE/AHS/ASC Structures, Structural Dynamics, and Materials Conference, Orlando, FL, Apr. 12-15, 2010.

[14] Truong, K., Yeo, H., and Ormiston, R. A., "Investigation of Finite Element Approaches for Rotor Blade Structural Dynamics," 36th European Rotorcraft Forum, Paris, France, Sept. 7-9, 2010.

[15] Berdichevsky, V. L., "Variational-Asymptotic Method of Constructing a Theory of Shells," *PMM*, Vol. 43, No. 4, 1979, pp. 664-687.

[16] Hodges, D. H., Atilgan, A. R., Cesnik, C. E. S., and Fulton, M. V., "On a Simplified Strain Energy Function for Geometrically Nonlinear Behavior of Anisotropic Beams," *Composites Engineering*, Vol. 2, No. 5-7, 1992, pp. 513-526.

[17] Cesnik, C. E. S. and Hodges, D. H., "Stiffness Constants for Initially Twisted and Curved Composite Beams," *Applied Mechanics Reviews*, Vol. 46, No. 11, Part 2, 1993, pp. S211-S220.

[18] Cesnik, C. E. S. and Hodges, D. H., "Variational-Asymptotical Analysis of Initially Twisted and Curved Composite Beams," *International Journal for Engineering Analysis and Design*, Vol. 1, No. 2, Apr. 1994, pp. 177-187.

[19] Ho, J. C., Yu, W., and Hodges, D. H., "Energy Transformation to Generalized Timoshenko Form by the Variational Asymptotic Beam Sectional Analysis," 51st AIAA/ASME/ASCE/AHS/ASC Structures, Structural Dynamics, and Materials Conference, Orlando, FL, Apr. 12-15, 2010.

[20] Yu, W., Volovoi, V. V., Hodges, D. H., and Hong, X., "Validation of the Variational Asymptotic Beam Sectional Analysis (VABS)," *AIAA Journal*, Vol. 40, No. 10, Oct. 2002, pp. 2105-2113.

[21] Kovvali, R. K., and Hodges, D. H., "Verification of the Variational Asymptotic Beam Section (VABS) Analysis for Initially Curved and Twisted Beams," *Journal of Aircraft*, Vol. 49, No. 3, May-June 2012, pp. 861-869.

[22] Popescu, B. and Hodges, D. H., "Asymptotic Treatment of the Trapeze Effect in Finite Element Cross-Sectional Analysis of Composite Beams," *International Journal of Nonlinear Mechanics*, Vol. 34, No. 4, 1999, pp. 709-721.

[23] Hopkins, A. S., and Ormiston, R., "An Examination of Selected Problems in Rotor Blade Structural Mechanics and Dynamics," *Journal of the American Helicopter Society*, Vol. 51, No. 1, Jan. 2006, pp. 104-119.

[24] Ortun, B., Petot, D., Truong, V. K., and Ohayon, R., "Towards a new generation of rotorcraft comprehensive analysis; coupling with CSM and CFD," 34th European Rotorcraft Forum, Liverpool, United Kingdom, Sept. 16-18, 2008.

[25] Epps, J. J., and Chandra, R., "The Natural Frequencies of Rotating Composite Beams with Tip Sweep," *Journal of the American Helicopter Society*, Vol. 41, No. 1, Jan. 1996, pp. 29-36.

[26] Hodges, D. H., Shang, X., and Cesnik, C. E. S., "Finite Element Solution of Nonlinear Intrinsic Equations for Curved Composite Beams," *Journal of the American Helicopter Society*, Vol. 41, No. 4, Oct. 1996, pp. 313-321.

[27] Maier, T. A., Sharp, D. L., and Abrego, A. I., "Aeroelastic Stability for Straight and Swept-Tip Rotor Blades in Hover and Forward Flight," American Helicopter Society 55th Annual Forum Proceedings, Montreal, Canada, May 25-27, 1999.

[28] Hodges, D. H., Ho, J. C., and Yu, W., "The Effect of Taper on Section Constants for In-Plane Deformation of an Isotropic Strip," *Journal of Mechanics of Materials and Structures*, Vol. 3, No. 3, March 2008, pp. 425-440.

Table 1: Comparison of non-rotating first torsion frequency of aluminum beam.

	Clamped-free			Free-free		
	L = 20×c	L = 10×c	L = 5×c	L = 20×c	L = 10×c	L = 5×c
Analytical solution, Hz	201.54	403.08	806.17	403.08	806.17	1612.34
RCAS NLB, Hz	201.54	403.08	806.17	403.08	806.17	1612.34
RCAS GCB, Hz	201.54	403.08	806.17	403.08	806.17	1612.34
MSC/Marc, Hz	204.41	412.93	842.36	404.41	810.29	1624.22
Difference, %	1.42	2.44	4.49	0.33	0.51	0.74

Table 2: Comparison of non-rotating third flap frequency of aluminum beam.

	Clamped-free			Free-free		
	L = 20×c	L = 10×c	L = 5×c	L = 20×c	L = 10×c	L = 5×c
Analytical solution, Hz	103.42	413.68	1654.73	202.67	810.67	3242.67
RCAS NLB, Hz	103.36	412.94	1641.87	202.42	806.75	3181.27
RCAS GCB, Hz	103.20	410.28	1603.10	202.00	800.40	3089.55
MSC/Marc, Hz	104.00	413.94	1623.61	202.33	804.37	3121.33
Difference, %	0.78	0.89	1.28	0.16	0.50	1.03

Table 3: Material properties of ADM rotor blade

Component	Material	Density lb sec^2/in^4	E11 lb/in^2	E22 lb/in^2	G12 = G13 lb/in^2	ν_{12}
Component 1 & 4	fiberglass +45°/-45°	1.5976E-04	1.6150E+06	1.6150E+06	6.6079E+05	0.46
Component 2	carbon graphite	1.3470E-04	2.0069E+07	1.2993E+06	5.0299E+05	0.30
Component 3 & 5	fiberglass 0°/90°	1.5976E-04	2.2769E+06	2.2769E+06	3.9662E+05	0.18
Component 6	tantalum	1.2804E-03	2.0972E+05	2.0972E+05	7.2292E+04	0.49
Component 7	foam	1.7871E-05	1.1995E+04	1.1995E+04	4.9978E+03	0.20
Component 8	Fiberite HY-E 9048A1F	1.7094E-04	5.1860E+06	2.2375E+06	5.6594E+05	0.27
Component 9	foam	8.9343E-06	4.5034E+03	4.5034E+03	1.0000E+03	0.45

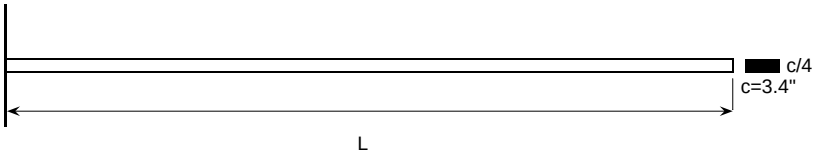

Fig. 1: Aluminum beam geometry

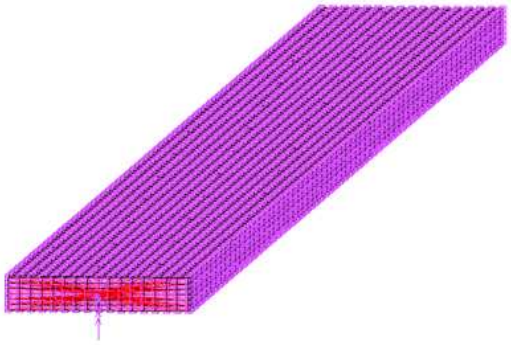

Fig. 2: 3-D mesh and clamped boundary condition for aluminum beam

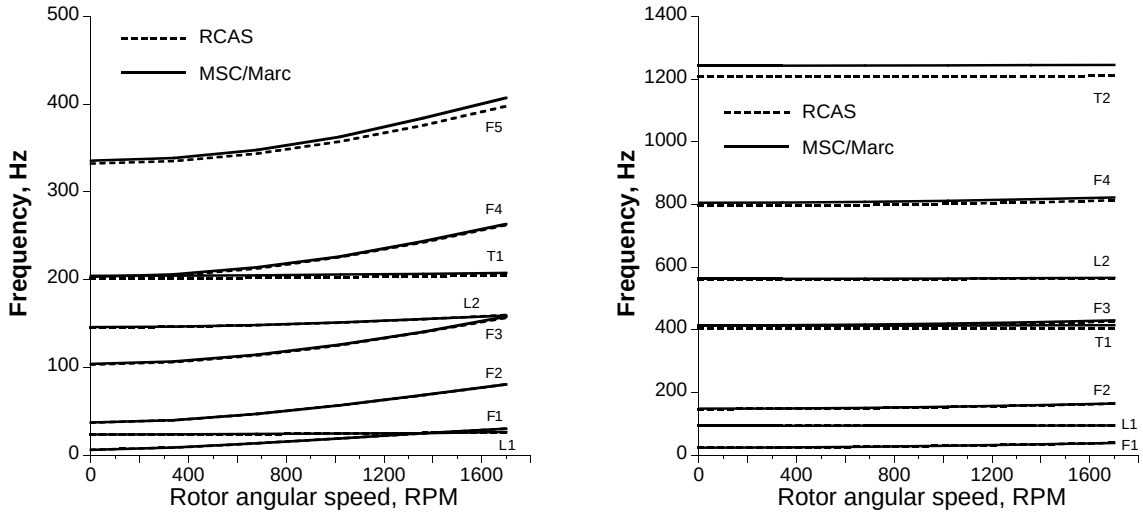

(a) L = 20×c (b) L = 10×c

Fig. 3: Frequency comparison for aluminum beam.

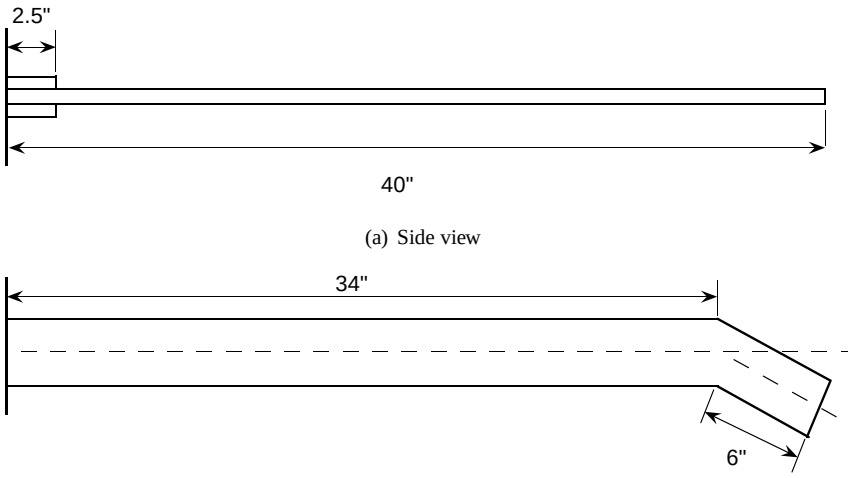

(a) Side view

(b) Top view

Fig. 4: Blade planform with tip sweep.

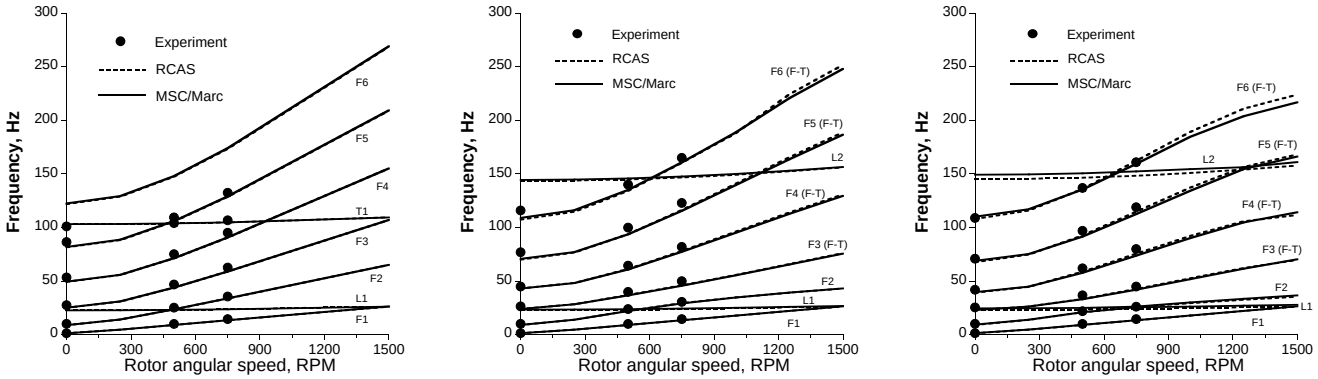

(a) 0-deg sweep (b) 30-deg sweep (c) 45-deg sweep

Fig. 5: Frequency comparison for aluminum beam with tip sweep.

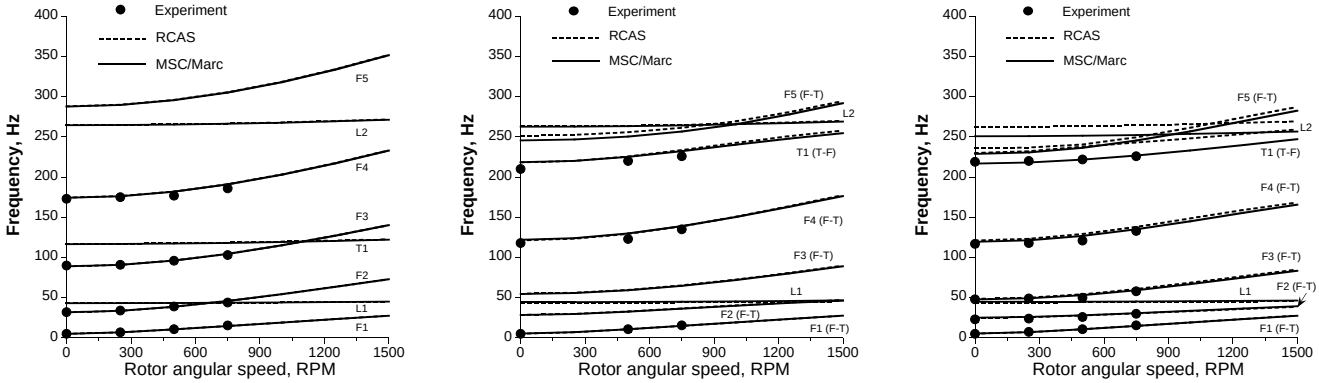

(a) 0-deg sweep (b) 30-deg sweep (c) 45-deg sweep

Fig. 6: Frequency comparison for graphite-epoxy beam with tip sweep, $[0^\circ]_{24}$.

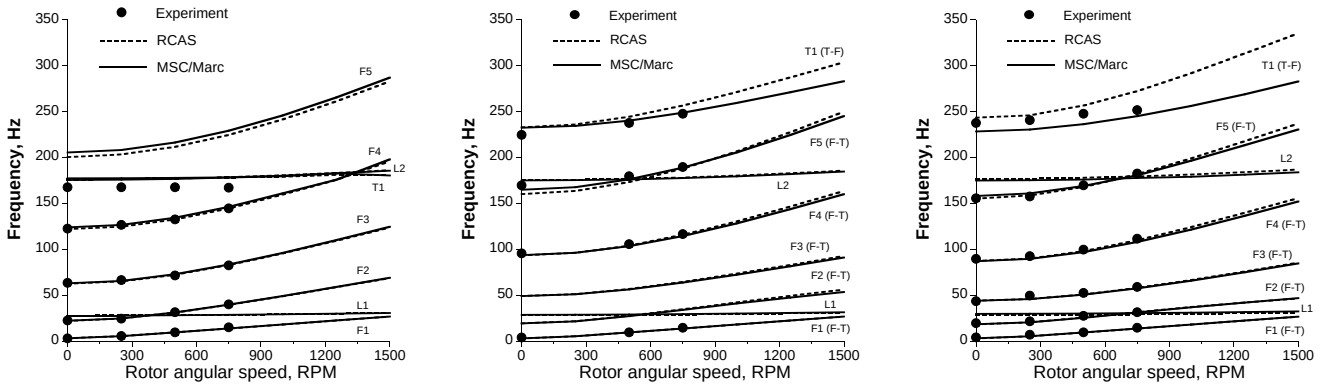

(a) 0-deg sweep (b) 30-deg sweep (c) 45-deg sweep

Fig. 7: Frequency comparison for graphite-epoxy beam with tip sweep, $[15^\circ]_{24}$.

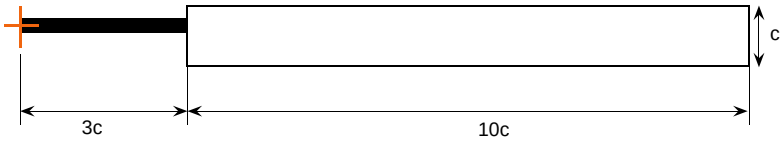

(a) Straight blade planform

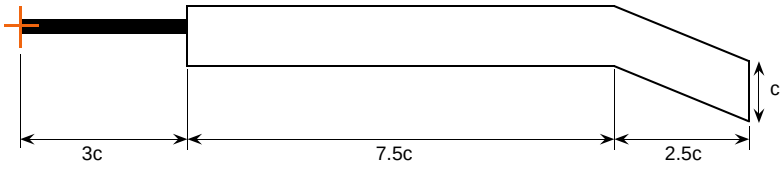

(b) Swept blade planform

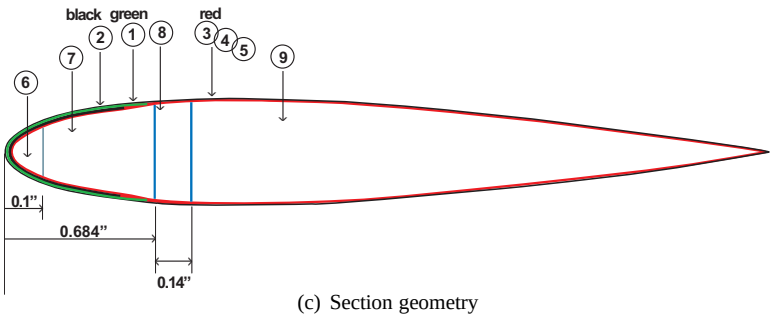

(c) Section geometry

Fig. 8: ADM rotor blade configuration.

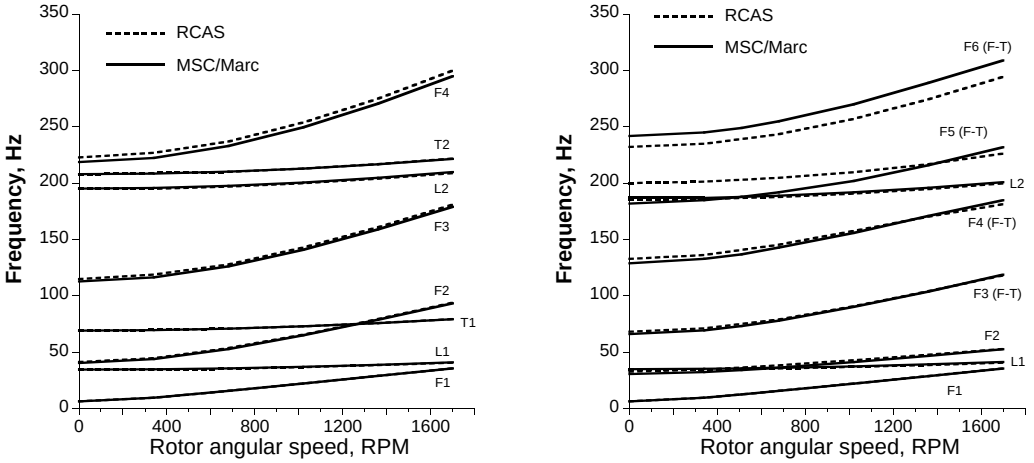

(a) 0-deg sweep (b) 28-deg sweep

Fig. 9: Frequency comparison for ADM rotor blade.

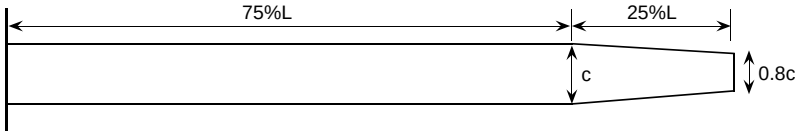

Fig. 10: Blade planform with tapered tip.

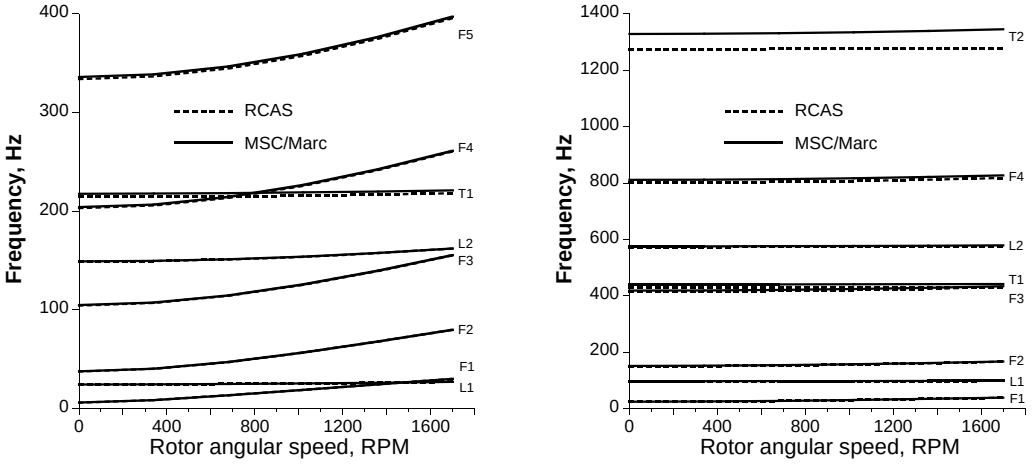

(a) L = 20 c (b) L = 10 c

Fig. 11: Frequency comparison for tapered aluminum beam.

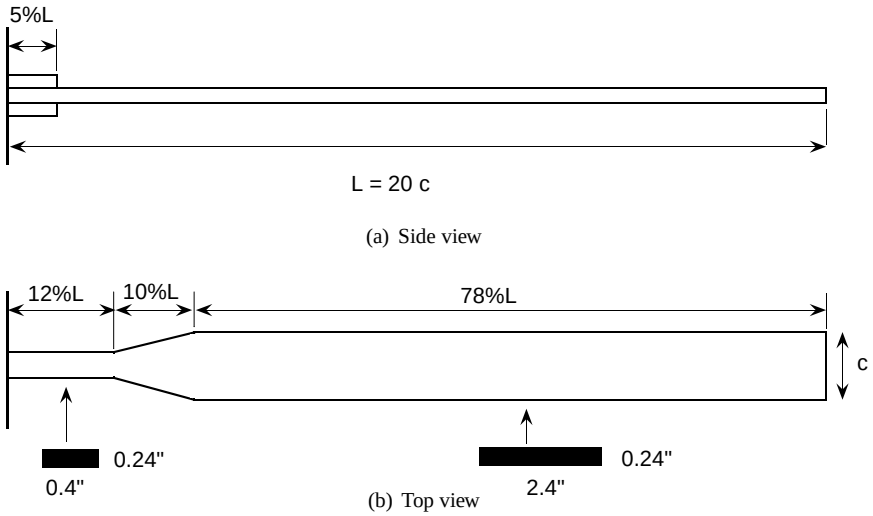

(a) Side view

(b) Top view

Fig. 12: Blade planform with inboard transition.

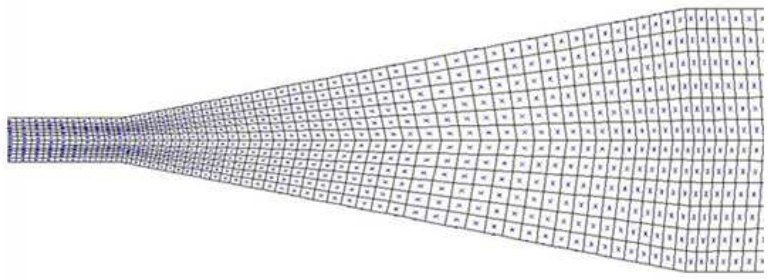

Fig. 13: 3-D modeling of beam with inboard transition.

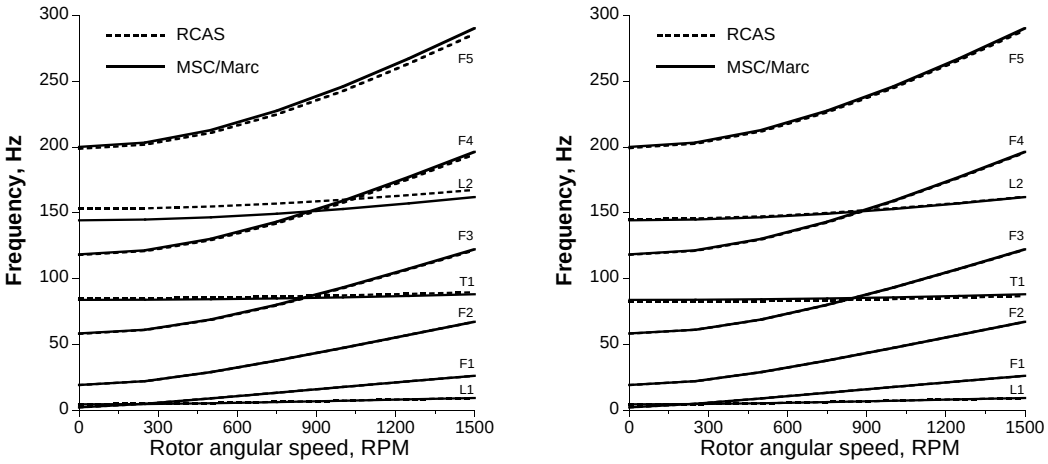

(a) RCAS with 12 elements (1 el, 1 el, 10 el)

(b) RCAS with 30 elements (4 el, 16 el, 10 el)

Fig. 14: Frequency comparison for aluminum beam with inboard transition.

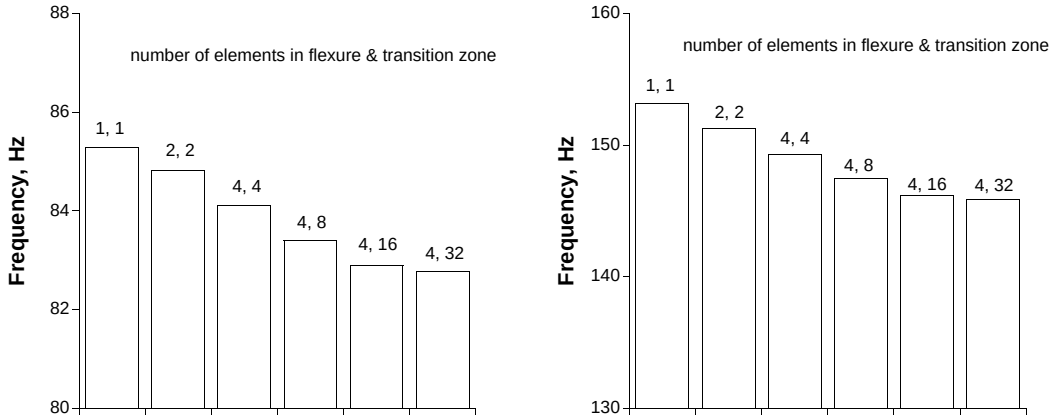

(a) first torsion frequency (b) second lag frequency

Fig. 15: Effects of number of elements on non-rotating frequencies for aluminum beam with inboard transition.

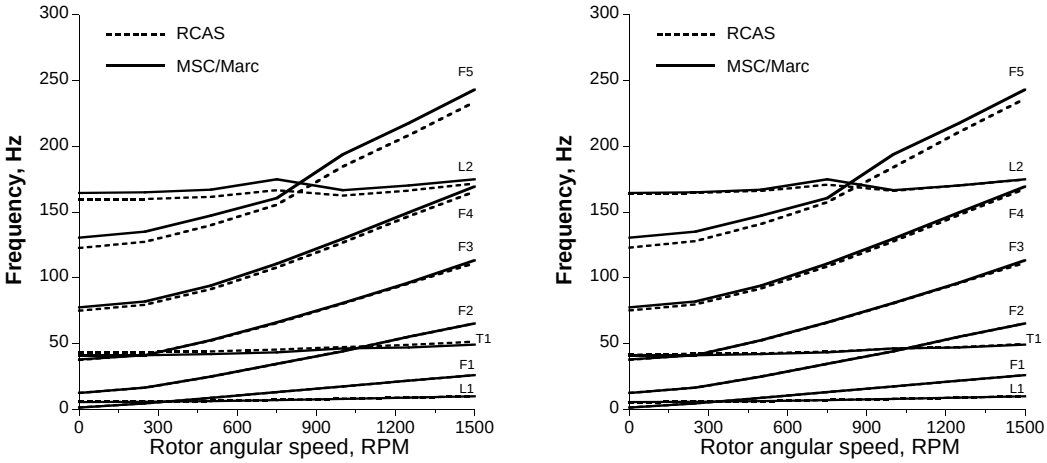

(a) RCAS with 12 elements (1 el, 1 el, 10 el) (b) RCAS with 30 elements (4 el, 16 el, 10 el)

Fig. 16: Frequency comparison for graphite-epoxy beam with inboard transition, $[15^\circ]_{24}$.